

1 Overview of STAR Results at Hard Probes 2020

2 **Zaochen Ye (for the STAR Collaboration)^{a,*}**

3 ^a*Rice University,*

4 *6100 Main Street, Houston, Texas, 77005, USA*

5 *E-mail: zaochen.ye@rice.edu, zaochen.ye.2017@gmail.com*

6 The STAR collaboration has presented latest measurements at this Hard Probes Conference which advance our knowledge of heavy-ion physics in various aspects. In this overview talk, I have presented the highlights of STAR results on behalf of the STAR collaboration. These results are presented in 15 parallel talks, 1 flash talk and 4 posters, and could be classified into 3 major categories in terms of probe types: 1) jet production; 2) heavy flavor production; 3) electroweak probes. In these proceedings, selected STAR results presented in this conference will be discussed. For more information, please refer to relevant presentations and proceedings from STAR for this conference.

HardProbes2020

1-6 June 2020

Austin, Texas

*Speaker

7 1. Jet production

8 Figure 1 shows the nuclear modification factor R_{CP} ((0-10%)/(60-80%)) of charged jet as a
 9 function of jet transverse momentum p_T for jet radius $R = 0.2$ and $R = 0.3$ in Au+Au collisions at
 10 $\sqrt{s_{NN}} = 200$ GeV [1]. The measured R_{CP} has no clear R or $p_{T,jet}^{ch}$ dependence at RHIC. The magnitude
 11 of R_{CP} measured at RHIC [1] is similar to that at LHC [2], although they are measured at different
 12 $p_{T,jet}^{ch}$ intervals. The magnitude of charged-hadron R_{CP} at RHIC [3] is also similar to that at LHC
 13 [4] in the overlapping p_T regions. While comparing the R_{CP} of the charged hadrons and charged
 14 jets, the significant rising trend of the charged-hadron R_{CP} at high p_T is not observed in the charged
 15 jet R_{CP} . The correlation between the hadron p_T and its parent jet p_T reflects the fragmentation
 16 process, which may result in a different p_T dependence of R_{CP} for the charged hadrons and jets.
 17 Thus, the combined measurements could provide new constraints on the theoretical treatments of
 18 jet quenching.

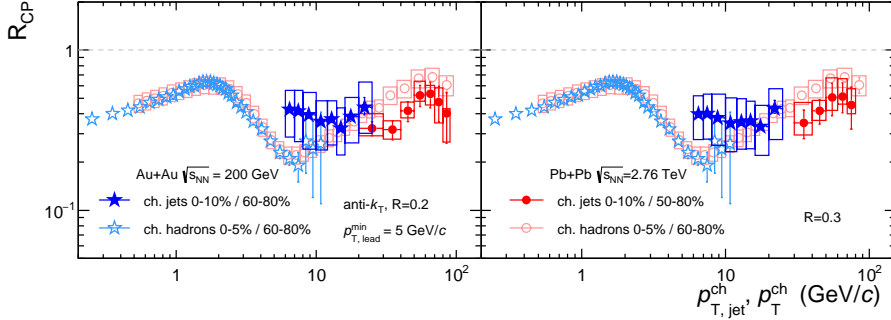


Figure 1: (Color online) R_{CP} of inclusive charged jets in Au+Au collisions at $\sqrt{s_{NN}} = 200$ GeV (solid blue stars) [1], compared to that measured in Pb+Pb collisions at $\sqrt{s_{NN}} = 2.76$ TeV (solid red dots) [2], for $R = 0.2$ and $R = 0.3$. The R_{CP} of inclusive charged hadrons from RHIC (blue open stars) [3] and LHC (red open circles) [4] are also shown. The vertical bars (boxes) denote the statistical (systematic) uncertainties.

19 Measurements of jets recoiling from highly energetic direct γ and π^0 triggers allow the study
 20 of parton flavor dependence (quarks vs. gluons) of jet suppression. Furthermore, γ_{dir} does not
 21 interact strongly with the medium, and it could be emitted from everywhere in medium while the
 22 π^0 triggers are mainly emitted from the surface of the medium. Thus the average path length of
 23 the recoil jets from π^0 triggers is expected to be larger than those from γ triggers [5]. Figure 2
 24 shows the ratio of recoil charged jet yields in Au+Au collisions to that in p+p collisions (simulated
 25 by PYTHIA 8), denoted as $I_{AA}^{PYTHIA-8}$, as a function of p_T for γ and π^0 triggers. The recoil jets
 26 from both triggers show similar suppression for $R = 0.2$ and a smaller suppression for $R = 0.5$,
 27 indicating broadening of recoil jets. However, a further study shows that the ratio of recoil jet yields
 28 from π^0 triggers for $R = 0.2$ to that for $R = 0.5$ can be reproduced by the PYTHIA 6 simulations,
 29 which indicates no significant in-medium broadening of recoil jets. Thus the current conclusion of
 30 in-medium jet broadening is still sensitive to the PYTHIA reference used. This will be resolved by
 31 the ongoing measurements in p+p collisions.

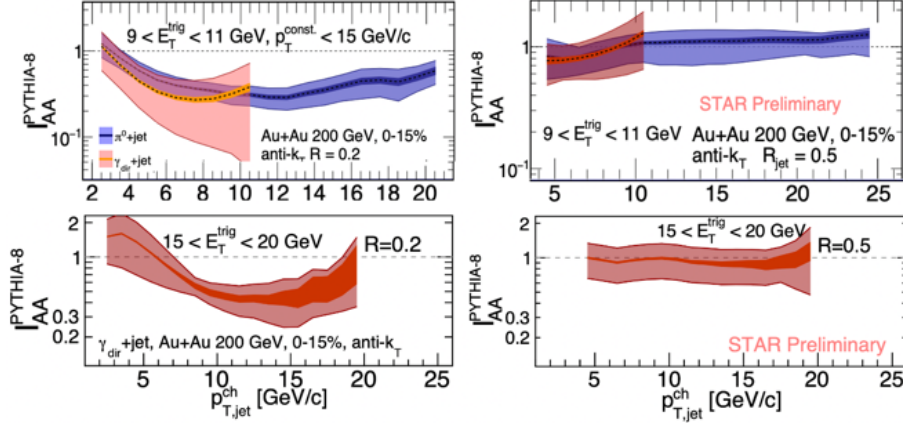


Figure 2: (Color online) Upper: $I_{AA}^{\text{PYTHIA-8}}$ as a function of $p_{T,jet}^{\text{ch}}$ of the charged jets recoiling from π^0 (blue) and γ_{dir} (red) triggers within $9 < E_T^{\text{trig}} < 11$ GeV/c. Lower: $I_{AA}^{\text{PYTHIA-8}}$ as a function of $p_{T,jet}^{\text{ch}}$ of the charged recoil jets triggered by γ_{dir} within $15 < E_T^{\text{trig}} < 20$ GeV/c. Left and right panels are for $R = 0.2$ and $R = 0.5$ jets, respectively. Dark (light) bands represent the statistical (systematic) uncertainties.

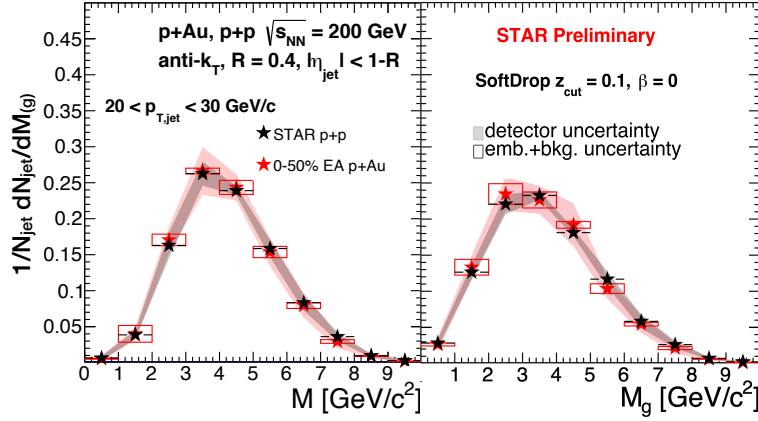


Figure 3: (Color online) Distributions of inclusive jet mass (M , left) and groomed jet mass (M_g , right) in p+p collisions (black stars) compared to those in p+Au collisions at $\sqrt{s_{NN}} = 200$ GeV. The gray bands denote the common uncertainty between p+p and p+Au data. The boxes denote the uncertainties from embedding and background assessed in p+Au data.

32 Jet mass is a good proxy of the parton virtuality, and provides important constraints on the
 33 theoretical treatments of the parton shower and hadronization processes. Figure 3 shows the
 34 measurements of the inclusive jet mass and groomed jet mass in p+Au (0-50% EA) and p+p
 35 collisions at 200 GeV, where EA is the event activity defined by the deposited energy in the inner
 36 Beam-Beam Counter in the Au-going direction at $-5 < \eta < -3.4$. The groomed jet mass is
 37 calculated by removing non-perturbative radiation with the SoftDrop grooming technique [6]. As
 38 the data show, both the jet mass and groomed jet mass in high EA p+Au collisions are consistent
 39 with those measured in p+p collisions within uncertainties, suggesting that the jet structure is not
 40 modified by the cold nuclear matter effects. This observation provides an important baseline for
 41 future jet mass measurements in Au+Au collisions.

2. Heavy flavor production

The large data sets taken in 2014 and 2016 for Au+Au collisions at $\sqrt{s_{NN}} = 200$ GeV with the Heavy Flavor Tracker (HFT) allow the separation of electrons from bottom and charm semileptonic decays at STAR. The left panel of Fig. 4 shows the R_{AA} of bottom and charm decayed electrons and their ratio as a function of electron p_T . The R_{AA} of electrons from bottom decays is systematically larger than that for electrons from charm decays. A constant fitting to the ratio gives a value of $1.90 \pm 0.25(stat.) \pm 0.21(syst.)$, which is above unity at a 3σ level. This provides a strong evidence for the mass hierarchy of the parton energy loss at RHIC.

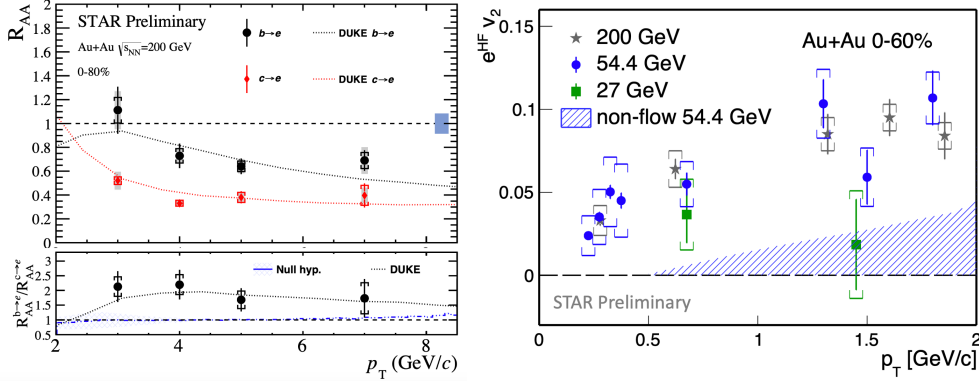


Figure 4: (Color online) Left panel shows R_{AA} of bottom and charm decayed electrons and their ratio as a function of electron p_T in Au+Au collisions at $\sqrt{s_{NN}} = 200$ GeV. Theoretical calculations from Duke model are shown as dotted curves [10]. Right panel shows the v_2 of heavy-flavor decayed electrons measured in Au+Au collisions at $\sqrt{s_{NN}} = 54.4$ GeV (blue dots) and 27 GeV (green squares) compared to STAR published data in 200 GeV (gray stars) [7]. The vertical bars (brackets) denote the statistical (systematic) uncertainties.

Due to the low production rate of heavy flavor quarks, measurements of their properties in heavy-ion collisions are challenging at low collision energies. Thanks to the large datasets taken in 2017 and 2018 for Au+Au collisions, we are able to perform the first precise measurements of heavy-flavor decayed electron elliptic flow v_2 at 54.4 GeV and 27 GeV at RHIC. As the right panel of Fig. 4 shows, the v_2 of heavy-flavor decayed electrons in Au+Au collisions at $\sqrt{s_{NN}} = 54.4$ GeV (blue dots) is comparable to that of STAR previous published results at $\sqrt{s_{NN}} = 200$ GeV (dark stars) [7]. This indicates that the heavy flavor quarks experience a similar collectivity at 54.4 GeV as at top RHIC energy. The results from Au+Au collisions at $\sqrt{s_{NN}} = 27$ GeV are shown as green squares, with a hint of smaller heavy-flavor decayed electron v_2 than those from 54.4 GeV and 200 GeV.

HFT also allows the direct reconstruction of open-charm mesons at STAR. In 2019 STAR reported that D^0 mesons are significantly suppressed in Au+Au collisions with respect to p+p collisions at $\sqrt{s_{NN}} = 200$ GeV [8]. Figure 5 shows recent measurements of the yield ratios of D^\pm and D_s^\pm to D^0 . The $(D^+ + D^-)/(D^0 + \bar{D}^0)$ yield ratio is consistent with PYTHIA 8 calculation, indicating that D^\pm experiences a similar level of suppression as D^0 in the Au+Au collisions. On the other hand, the $(D_s^+ + D_s^-)/(D^0 + \bar{D}^0)$ yield ratio is significantly higher than the PYTHIA 8 calculation for all applicable p_T region and in different centrality bins, consistent with the expectation of coalescence hadronization of charm quarks with enhanced strange quarks [9].

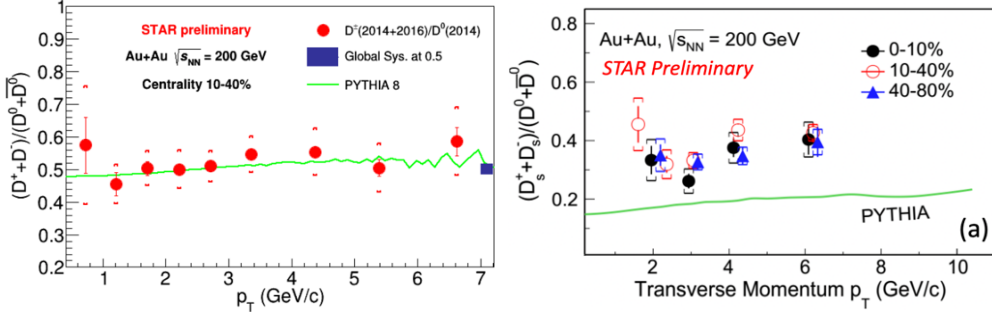


Figure 5: (Color online) The ratio of $(D^+ + D^-)/(D^0 + \bar{D}^0)$ (left panel) and $(D_s^+ + D_s^-)/(D^0 + \bar{D}^0)$ (right panel) as a function of p_T measured in Au+Au collisions at $\sqrt{s_{NN}} = 200$ GeV, compared to PYTHIA 8 calculations (green curves). The vertical bars and brackets denote the statistical and systematic uncertainties, respectively.

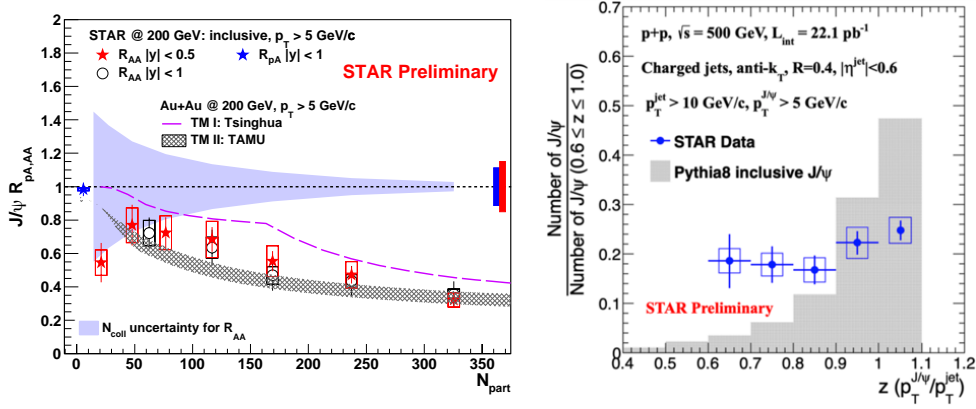


Figure 6: (Color online) The left panel shows the R_{pA} of inclusive J/ψ (blue star) compared to the STAR published R_{AA} (open circles [11] and red stars [12]). The right panel shows the z distribution of inclusive J/ψ meson produced within a jet (blue dots) measured in p+p collisions at $\sqrt{s} = 200$ GeV compared to the PYTHIA8 calculation (gray filled histogram). The vertical bars and boxes denote the statistical and systematic uncertainties, respectively.

68 The latest J/ψ R_{pA} at high p_T ($p_T > 5$ GeV/c) measured with the data taken in 2015 for p+p
 69 and p+Au collisions, shown as the blue star in the left panel of Fig. 6, is consistent with unity.
 70 This indicates that the strong suppression of high p_T J/ψ observed in Au+Au collisions (open
 71 circles and red stars) [11, 12] is dominantly due to the hot nuclear matter effects instead of the cold
 72 nuclear matter effects. Although the J/ψ meson was discovered more than four decades ago, its
 73 production mechanism still remains a mystery. A recent theoretical work suggests that measuring
 74 J/ψ production in jets could help distinguish different J/ψ production mechanisms, and potentially
 75 be used to constrain the long-distance-matrix-elements, a set of supposedly universal constants,
 76 in the NRQCD calculations [13]. The first measurement of J/ψ in jets at RHIC is shown in the
 77 right panel of Fig. 6, which shows a clearly different trend of $z(J/\psi)$ compared to that from the
 78 leading-order NRQCD-based PYTHIA 8 calculation. This indicates the J/ψ production in jets is
 79 less isolated in data than the PYTHIA 8 prediction.

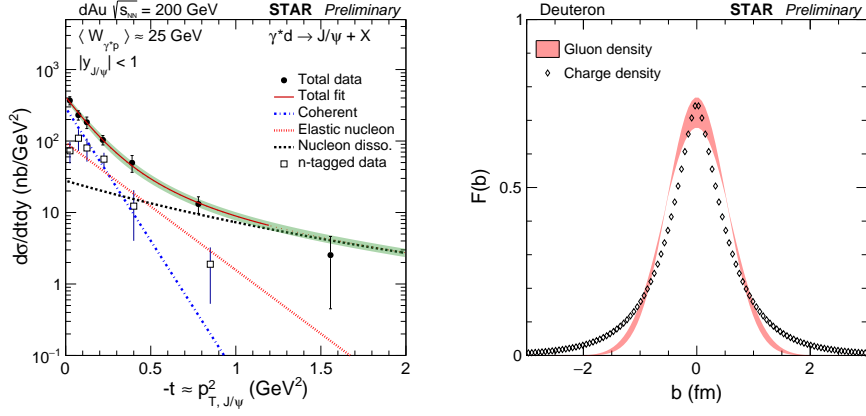


Figure 7: (Color online) The differential cross sections of photo-produced J/ψ off the deuteron as a function of p_T^2 of J/ψ (black dots for inclusive data, open squares for neutron tagged data) are shown in the left panel. The contributions of coherent diffractive production, incoherent diffractive production (elastic) and the nucleon dissociations are shown in dotted curves. The gluon density $F(b)$ as a function of the impact parameter b is compared to the charge density distribution as shown in the right panel.

80 J/ψ production in the ultra-peripheral collisions (UPC) probes the gluon density distributions
 81 inside the nucleons and nuclei. The left panel of Fig. 7 shows the differential cross section $d\sigma/dt$ of
 82 photo-produced J/ψ off the deuteron as a function of the momentum transfer $-t$ (approximated by
 83 the p_T^2 of J/ψ) with a photon-nucleon center-of-mass energy $\langle W_{\gamma^*p} \rangle \approx 25$ GeV. Data are shown as
 84 black dots, which include three main contributions: the coherent diffractive production, incoherent
 85 diffractive production without breaking the nucleon, and the nucleon dissociation. By performing
 86 the template fitting of different contributions, the slope of the coherent diffractive component is
 87 extracted, which is closely related to the deuteron size. The gluon density $F(b)$ as a function of the
 88 impact parameter b is extracted by a Fourier transformation based on the slope parameter, and is
 89 shown as the gray band in the right panel of Fig. 7. It is found to be wider than the charge density
 90 distribution of the deuteron (shown in the same figure).

91 3. Electroweak probes

92 Dilepton production has been proposed as an excellent probe to the chiral symmetry restoration
 93 and the thermal properties of the hot medium produced in the heavy-ion collisions. The large Au+Au
 94 datasets taken at 54.4 GeV (2017) and 27 GeV (2018) greatly improve the precision of the dielectron
 95 measurements at these collision energies. The ratios of measured dielectron invariant mass spectra
 96 to the cocktail in Au+Au collisions at $\sqrt{s_{NN}} = 27$ GeV and 54.4 GeV are shown in the top two panels
 97 of Fig. 8. The ongoing analyses with these two datasets and the future analyses using the datasets
 98 from STAR BES-II will allow us to study the in-medium modification of ρ vector meson for p_T ,
 99 centrality and beam-energy dependences, and carry out a potential temperature measurement from
 100 the thermal radiation in the intermediate mass region ($M_\phi < M_{ee} < M_{J/\psi}$, where an enhancement
 101 to cocktail is indicated in 27 GeV data as shown in Fig. 8a).

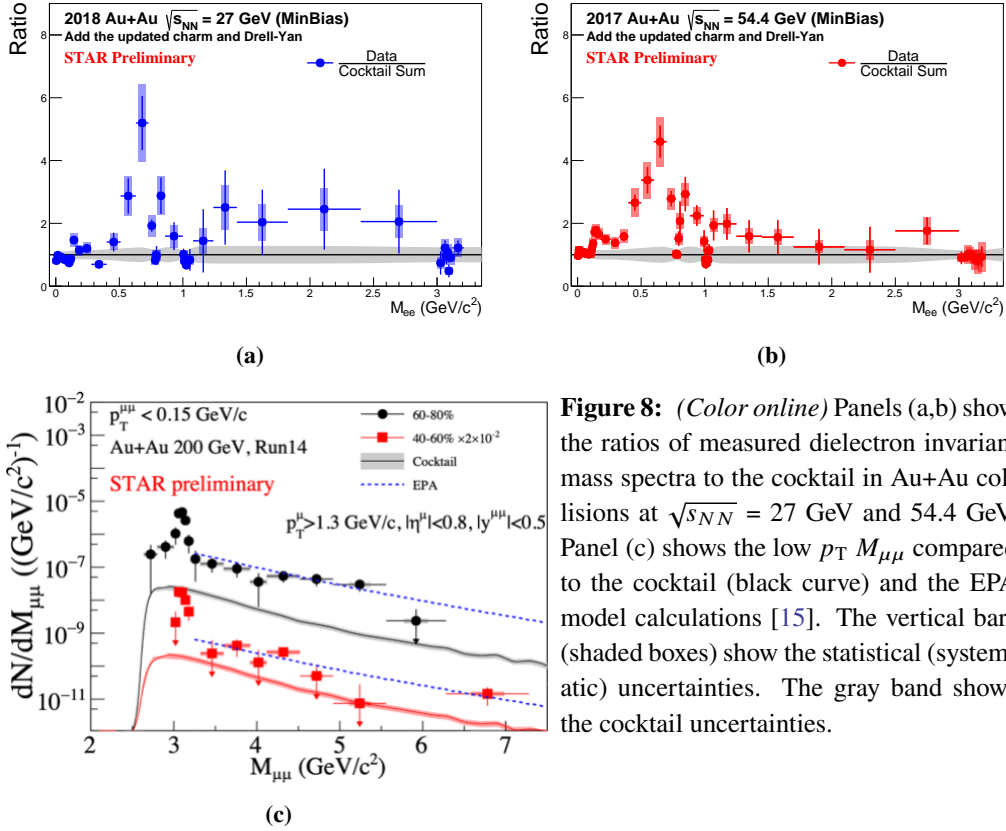


Figure 8: (Color online) Panels (a,b) show the ratios of measured dielectron invariant mass spectra to the cocktail in Au+Au collisions at $\sqrt{s_{NN}} = 27$ GeV and 54.4 GeV. Panel (c) shows the low p_T $M_{\mu\mu}$ compared to the cocktail (black curve) and the EPA model calculations [15]. The vertical bars (shaded boxes) show the statistical (systematic) uncertainties. The gray band shows the cocktail uncertainties.

102 In 2018, STAR reported the first measurement of the e^+e^- pair enhancement compared to the
 103 cocktail in the mass region of $0.4 < M_{ee} < 2.6$ GeV/c² at very low p_T ($p_T < 0.15$ GeV/c) region
 104 in non-central Au+Au collisions at $\sqrt{s_{NN}} = 200$ GeV and U+U collisions at $\sqrt{s_{NN}} = 193$ GeV [14].
 105 This enhancement was found to be consistent with the expectation of the photon-photon interactions
 106 in these collisions. The data taken in 2014 for Au+Au collisions at $\sqrt{s_{NN}} = 200$ GeV with the Muon
 107 Telescope Detector (MTD) allow a study of the same physics process using low- p_T $\mu^+\mu^-$ pairs. The
 108 new measurements shown in Fig. 8c exhibit the similar enhancement as in e^+e^- pairs, extending to
 109 a higher mass range of $3.2 < M_{ee} < 7.5$ GeV/c². The observed enhancement can be well described
 110 by the equivalent photon approximation model calculation [15].

111 4. Summary and Outlook

112 In this conference, STAR has presented latest results from different collision systems (p+p,
 113 p+Au and Au+Au) and different collision energies from 500 GeV for p+p collisions down to 27
 114 GeV for Au+Au collisions. The main upgrades of the STAR experiment in the BES-II program
 115 include the inner TPC sectors (iTPC), the Event Plane detector (EPD) and the end-cap Time Of
 116 Flight detector (eTOF), installed in the last three years. They improve and extend STAR's tracking
 117 and particle identification capabilities to lower p_T and higher η , and enable the determination of
 118 the event plane at forward rapidity. While the data taking of BES-II is still ongoing, data analyses
 119 have already started and the physics results will be delivered soon. After twenty years of successful

120 operation, STAR still keeps evolving with new upgrades. The next upgrades will happen at the
121 forward ($2.5 < \eta < 4$) region beyond 2021, consisting of trackers (silicon microstrip tracker and
122 small-strip Thin Gap Chamber) and calorimeters (ECAL and HCAL). These upgrades will allow us
123 to study the proton spin structure, Drell-Yan process, direct photon production, jet correlation and
124 offer unique capability for investigating the origin of Λ global polarization in Au+Au collisions.

125 References

- 126 [1] J. Adam *et al.* [STAR], [arXiv:2006.00582 [nucl-ex]].
127 [2] B. Abelev *et al.* [ALICE], JHEP **03**, 013 (2014) [arXiv:1311.0633 [nucl-ex]].
128 [3] J. Adams *et al.* [STAR], Phys. Rev. Lett. **91**, 172302 (2003) [arXiv:nucl-ex/0305015 [nucl-ex]].
129 [4] G. Aad *et al.* [ATLAS], JHEP **09**, 050 (2015) [arXiv:1504.04337 [hep-ex]].
130 [5] L. Adamczyk *et al.* [STAR], Phys. Lett. B **760**, 689-696 (2016) [arXiv:1604.01117 [nucl-ex]].
131 [6] A. J. Larkoski, S. Marzani, G. Soyez and J. Thaler, JHEP **05**, 146 (2014) [arXiv:1402.2657
132 [hep-ph]].
133 [7] L. Adamczyk *et al.* [STAR], Phys. Rev. C **95**, no.3, 034907 (2017) [arXiv:1405.6348 [hep-ex]].
134 [8] J. Adam *et al.* [STAR], Phys. Rev. C **99**, no.3, 034908 (2019) [arXiv:1812.10224 [nucl-ex]].
135 [9] M. He, R. J. Fries and R. Rapp, Phys. Rev. Lett. **110**, no.11, 112301 (2013) [arXiv:1204.4442
136 [nucl-th]].
137 [10] S. Cao, G. Y. Qin and S. A. Bass, Phys. Rev. C **92**, no.2, 024907 (2015) [arXiv:1505.01413
138 [nucl-th]].
139 [11] L. Adamczyk *et al.* [STAR], Phys. Lett. B **722**, 55-62 (2013) [arXiv:1208.2736 [nucl-ex]].
140 [12] J. Adam *et al.* [STAR], Phys. Lett. B **797**, 134917 (2019) [arXiv:1905.13669 [nucl-ex]].
141 [13] Z. B. Kang, J. W. Qiu, F. Ringer, H. Xing and H. Zhang, Phys. Rev. Lett. **119**, no.3, 032001
142 (2017) [arXiv:1702.03287 [hep-ph]].
143 [14] J. Adam *et al.* [STAR], Phys. Rev. Lett. **121**, no.13, 132301 (2018) [arXiv:1806.02295 [hep-
144 ex]].
145 [15] W. Zha, J. D. Brandenburg, Z. Tang and Z. Xu, Phys. Lett. B **800**, 135089 (2020)
146 [arXiv:1812.02820 [nucl-th]].